THE JOURNAL OF PHYSICAL CHEMISTRY A

Article

pubs.acs.org/JPCA

Scattering Dynamics, Survival, and Dispersal of Dimethyl Methylphosphonate Interacting with the Surface of Multilayer Graphene

K. D. Gibson and S. J. Sibener*

The James Franck Institute and Department of Chemistry, The University of Chicago, 929 East 57th Street, Chicago, Illinois 60637, United States

ABSTRACT: We explored the interaction of a molecular beam of dimethyl methylphosphonate with a multilayer graphene surface to better understand the fate of chemical warfare agents in the environment. The experiments were done at surface temperatures between 120 and 900 K and translational energies between 200 and 1500 meV. At the lowest temperatures, the dimethyl methylphosphonate is adsorbed, with the molecules next to the carbon surface held slightly more strongly than the bulk molecular film that grows with continued dosing. We measured the desorption energy for submonolayer coverage using modulated beam techniques and found a value of 290 meV (28 kJ/mol). At higher surface temperatures, where the residence times are very short, we measured the scattering of the dimethyl methylphosphonate as a function of angle and translational kinetic energy. For a surface temperature of 250 K, with translational kinetic energies between 200 and 1500 meV, much of the incident flux has nearly been accommodated by the surface temperature and has no memory of the incident momentum. The internal energy also seems to be at least partially accommodated. As the surface temperature increases, the scattering transitions to direct-inelastic reflection, where much of the incident translational energy is retained, and the intensity of the scattering peaks superspecularly toward glancing final angles. These results demonstrate the efficacy of using kinetic energy controlled molecular beams to probe the interactions of complex organic molecules with well-defined surfaces, extending our fundamental understanding of how the dynamics for such systems crossover from trapping−desorption to direct inelastic scattering. Moreover, these results indicate that simulations that model the dispersal of chemical warfare agents using common interfaces in the environment need to account for multiple bounce trajectories and survival of the impinging molecules.

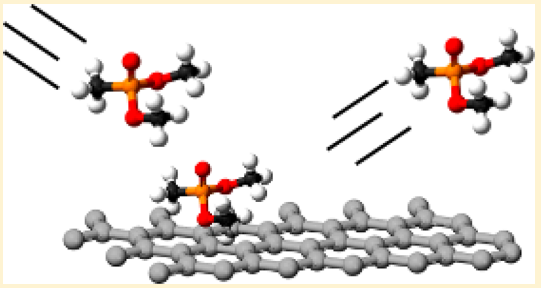

INTRODUCTION

Understanding the interaction of chemical warfare agents with environmental materials is of critical importance in understanding their dispersal and formulating ways for the neutralization of contaminated surfaces. Many of the most toxic nerve agents are the G-type and V-type agents, and all are organophosphorous compounds.[1] Because the actual agents are so toxic, most studies use a nontoxic simulant, often dimethyl methylphosphonate (DMMP). This is considered as a realistic simulant for the agent sarin (GB), having a similar vapor pressure and chemical bonding characteristics.[1,2]

Previous studies have dealt with reactive surfaces including metals,[3−6] oxides such as TiO_2 and Y_2O_3,[7−10] and supported catalysts.[7,11,12] These experiments were concerned with the neutralization and destruction of organophosphorus agents. In the event of a release of an agent into the environment, there will be many types of surfaces, several of which will be chemically inert; think of surfaces such as leaves, glass, concrete structures, roadways, or painted metals. The fate and dispersal of the agent is then of considerable interest. It can be reflected from the surface immediately, or if adsorbed, slowly evaporate. It can also be absorbed into the bulk or have sufficient surface residence time to interact with another adsorbed molecule, such as O_2.[13] It is also possible for the molecule to decompose at elevated temperatures. There have been few studies of adsorption and absorption of DMMP on relatively inert materials.[14,15] Hegde et al.[4] experimented with DMMP adsorbed onto cryogenically cooled Rh(100) and Rh(100) covered with a monolayer of carbon. Upon heating, some of the DMMP adsorbed on the initially clean Rh(100) decomposed. The same experiment with a carbon monolayer showed no evidence of DMMP decomposition, only desorption. Liang et al.[16] studied the thermal decomposition of DMMP in a heated SiC tube and found no measurable decomposition until the temperature of the tube was ∼1000 K.

Not only is the surface composition important, but also the interaction of molecules that are internally and translationally hot can be of interest. A brief perusal of the literature shows that many of the chemical warfare munitions have explosive delivery systems, so the initial contact with a surface may be from an

Special Issue: Piergiorgio Casavecchia and Antonio Lagana Festschrift

Received: December 18, 2015
Revised: February 4, 2016
Published: February 19, 2016

DOI: 10.1021/acs.jpca.5b12419
J. Phys. Chem. A 2016, 120, 4863−4871

energetic molecule. When it comes to the fate of chemical warfare agents under combat conditions or during decontamination of surfaces, the temperature of the surface can vary over a wide range, so that surface temperature effects also need to be studied.

For the experiments described in this paper, we grew multilayer graphene (MLG) on a Rh(111) surface, a surface that we expect to be fairly inert, and examined the adsorption and scattering of a molecular beam of DMMP at surface temperatures (T_S) between 120 and 900 K. The advantage of MLG over graphite was that we could easily and reproducibly grow a fresh surface when needed. We use a combination of temperature-programmed desorption (TPD), modulated beam scattering, and time-of-flight (TOF) measurements to examine the kinetics and dynamics of the DMMP−surface interactions. Further, the use of molecular beams allowed us to investigate the scattering of DMMP with well-defined translational energies from 200 to 1500 meV.

EXPERIMENTAL SECTION

The instrument used in this study is schematically depicted in Figure 1. A molecular beam was produced in the source chamber

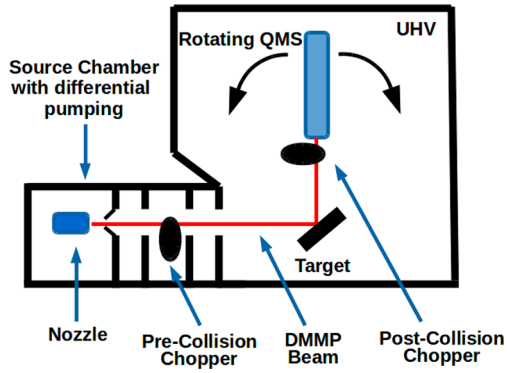

Figure 1. Schematic of the scattering machine.

and passed through several regions of differential pumping before entering an ultra-high-vacuum (UHV) chamber (base pressure of 2×10^{-10} Torr). The target was mounted on a manipulator that could be rotated with respect to the beam, giving a variable incident (polar) angle, θ_i. The target could be resistively heated to ∼1300 K, and cryogenically cooled. A differentially pumped quadrupole mass spectrometer (QMS) could independently rotate around the target so that the final angle (θ_f) was variable. The scattering plane is defined by the arc of this motion. The ions for the QMS are produced in an electron-bombardment detector, using 95 eV electrons. The cracking pattern of DMMP had a maximum signal at a mass-to-charge ratio (m/e) of 94 (the ratio of the m/e = 124 (parent) to m/e = 94 was ∼0.25) at a nozzle temperature of 333 K, consistent with the literature.[17] For most of the measurements, we monitored m/e = 94.

There were two mechanical choppers, one before and one after the target. The precollision chopper had a combination of narrow slots for measuring the incident translational energy via time-of-flight, and wide slots for square-wave modulation of the incident beam. The postcollision chopper had a cross-correlation (CC) pattern[18] and was attached to the detector so that it rotated with the mass spectrometer. The CC technique makes it possible to make precise TOF measurements with a 50% duty cycle, thus improving the signal acquired as compared to small (narrow) single slot pulses. Using a postcollision chopper allows for the measurement of molecular velocity independently of any surface residence time.

The molecular beam was produced by bubbling He or Ar through a reservoir of DMMP (Sigma-Aldrich, ≥97%, distilled before use), and then expanding through a 19 μm nickel pinhole supported in a stainless steel nozzle assembly. The reservoir was held at 303 K, and the nozzle at 333 K, to preclude any DMMP condensation. Most of these experiments were done using He with a backing pressure of 7 psia. This produced a beam having an average translational energy of 730 meV, with a $\Delta E/E$ = 0.4 full-width half-maximum, measured by lowering the target out of the beam path and rotating the detector so that it was exposed to the direct beam. We did not directly measure the DMMP flux. On the basis of our experience with other beams made in a similar manner in our laboratory, the low vapor pressure of DMMP (∼1 Torr at 303 K),[2] and the strength of the signal from the direct beam, allow us to estimate that the incident flux was less than 0.1 monolayers s^{-1}. We also used higher backing pressures for the supersonic expansion, which generated more intense beams with narrower energy distributions, but this led to high mass peaks in the mass spectrum (m/e = 218, 233) which we attribute to *DMMP clusters* (maybe dimers) in the beam. We were unable to make a beam with Ar as the carrier gas having sufficient intensity without some clustering. (We note that such clusters are of interest themselves given the role they play in the formation and dispersal of environmental aerosols.)

The target was a Rh(111) crystal upon which we grew the MLG. The technique used was to expose a clean 300 K surface to ethylene (beam dosing, flux $\sim 10^{-14}$ cm^{-2} s^{-1}),[19] heat to 1070 at 100 K/min, and then expose the surface to ethylene for 10 min. On cool down, a well-ordered graphene monolayer was formed.[19,20] Further exposing this surface to ethylene at a surface temperature (T_S) of 1170 K leads to the absorption of carbon, and then slowly cooling to 1000 K (10 K/min) causes the carbon to segregate to the surface of the metal and form an MLG overlayer.[21,22] The top panel of Figure 2 shows the Auger electron spectrum of the surface for ∼4 layer thick MLG. Coverage was calibrated by monitoring the attenuation of the Rh peak, using the monolayer graphene Auger spectra to calibrate the attenuation per layer, assuming layer-by-layer growth.[23] The bottom panel shows a He diffraction spectrum of this surface. This diffraction pattern indicates that the surface is well-ordered. There is still the presence of peaks due to the lattice mismatch between graphite and Rh(111). There is also a feature (indicated by the arrow) that is due to the graphene lattice. The top surface of the MLG is aligned with the Rh(111) crystallographic directions; the graphene lattice peak disappears when the crystal azimuth is changed relative to the scattering plane, providing clear evidence for alignment and the lack of mosaic texture in the overlayer. All of the MLG overlayers used in these experiments were ≥4 layers thick. Discussion of the He atom diffraction patterns can be found in a previous publication.[19]

RESULTS AND DISCUSSION

Figure 3 shows the TPD spectrum for DMMP adsorbed on MLG. The surface was exposed to DMMP at T_S = 125 K, and then the surface temperature was linearly ramped (10 K/min) while the m/e = 94 signal was monitored with the QMS. The results show two distinct desorption features similar to what was seen for DMMP adsorbed on a monolayer of carbon on Rh(100),[4] though at a lower surface temperature. As a function

DOI: 10.1021/acs.jpca.5b12419
J. Phys. Chem. A 2016, 120, 4863−4871

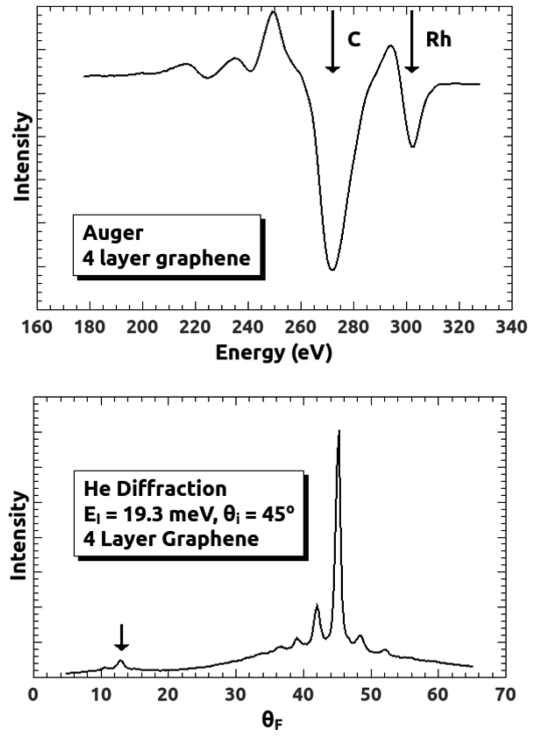

Figure 2. Top panel: Auger electron spectrum for 4 layer MLG. Bottom panel: He atom diffraction spectrum along the ⟨11⟩ direction of the Rh(111) surface (T_S = 200 K).

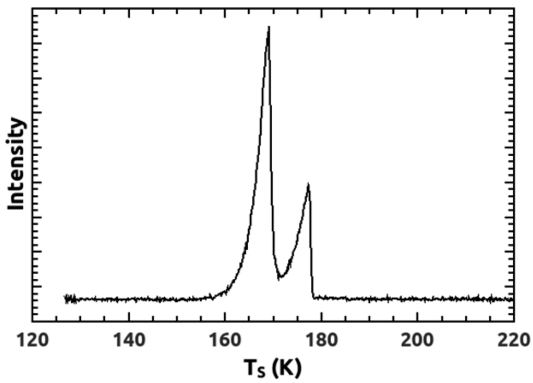

Figure 3. Temperature-programmed desorption spectrum of DMMP (m/e = 94). The surface was dosed with DMMP at T_S = 125 K, and then the temperature was linearly ramped at 10 K/min.

of dosing time, the adsorption state that leads to the higher temperature desorption feature fills in first but soon saturates, whereas the lower temperature state continues to be populated as dosing time is increased. The higher temperature feature is due to the formation of a monolayer on top of the carbon surface;[4] the DMMP is more strongly bound to the surface than to other DMMP molecules, wetting the surface. Subsequent adsorption is a multilayer on top of the already adsorbed DMMP monolayer.

To investigate the adsorption of DMMP further, we employed modulated molecular beam techniques.[24,25] We used a mechanical chopper to give the incident beam a square-wave modulation; an example spectrum is shown in Figure 4, where the modulation frequency was 25 Hz and the QMS was tuned to m/e = 94. For the fluxes used, the results are all for a submonolayer coverage. To analyze the data, we assumed simple desorption kinetics with a desorption rate proportional to

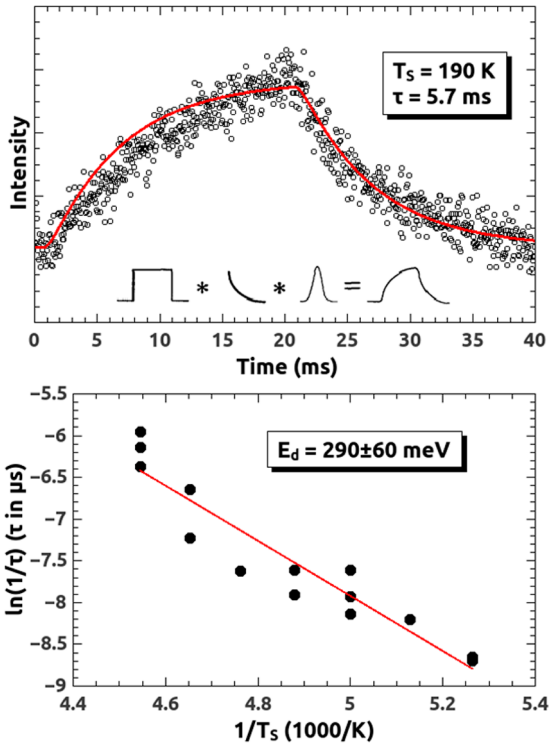

Figure 4. Top panel: example of a square-wave modulated beam experiment, with a chopping frequency of 25 Hz. The red line is from the fitting procedure, which is schematically shown in the inset (see text). Bottom panel: Arrhenius plot for all of the measurements.

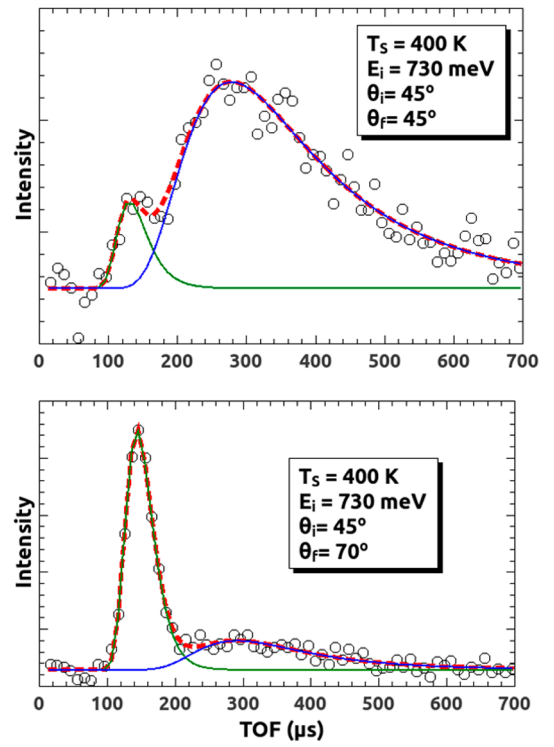

Figure 5. Example TOF spectra, taken using the postcollision chopper. As shown, they have been deconvoluted for the cross-correlation pattern. Each was fit with the sum of two shifted Maxwell−Boltzmann velocity distributions; the green and blue lines are the individual distributions, and the red line is their sum.

DOI: 10.1021/acs.jpca.5b12419
J. Phys. Chem. A 2016, 120, 4863−4871

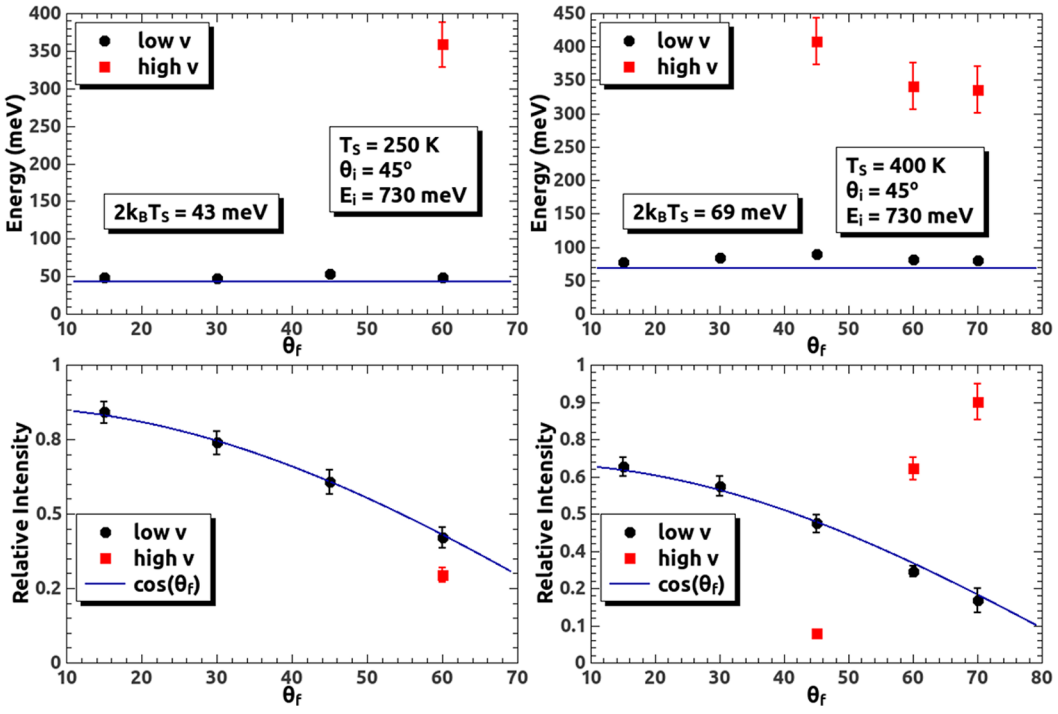

Figure 6. Top panels: average final translational energy as a function of θ_f. Bottom panels: scattered intensity as a function of θ_f. For any final angles where the TOF distributions were bimodal, two points are plotted, with the higher energy in red. The line through the intensities is $\cos(\theta_f)$. The blue lines in the energy plot are for $E = 2k_BT_S$.

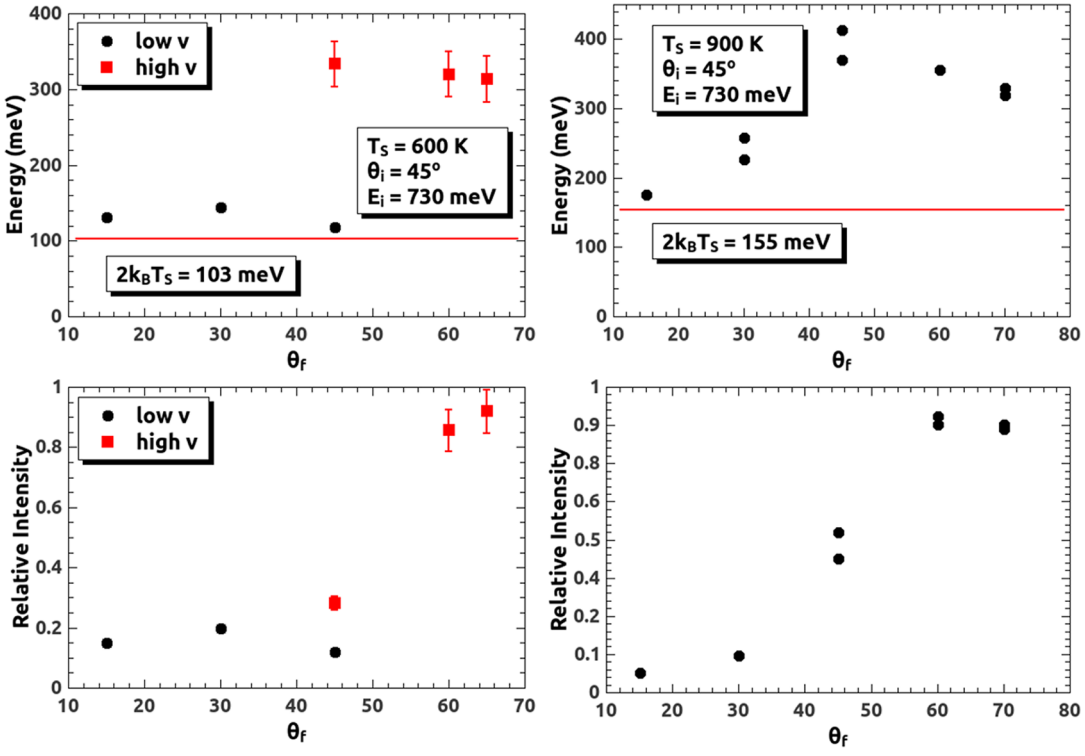

Figure 7. Top panel: average final translational energy as a function of θ_f. Bottom panels: scattered intensity as a function of θ_f. For any final angles where the TOF distributions were bimodal, two points are plotted, with the higher energy in red. The red lines in the energy plot are for $E = 2k_BT_S$.

$\exp[-t/\tau]$. A nonlinear least-squares routine was used to fit the data, where the model was a convolution of the square wave with the incident velocity distribution ($f(v_i)$), the final velocity distribution ($f(v_f)$), and the exponential decay, with τ as a variable. $F(v_i)$ was measured, and $f(v_f)$ was assumed to be a Maxwell−Boltzmann distribution with an $\langle E \rangle = 2k_BT_S$, where k_B is Boltzmann's constant. This assumption will be shown to be reasonable in the following discussion for the conditions of these experiments, where $\theta_i = 45°$ and $\theta_f = 15°$. The trailing edge of the spectra were fit well with this model if we restricted the fitting

DOI: 10.1021/acs.jpca.5b12419
J. Phys. Chem. A 2016, 120, 4863−4871

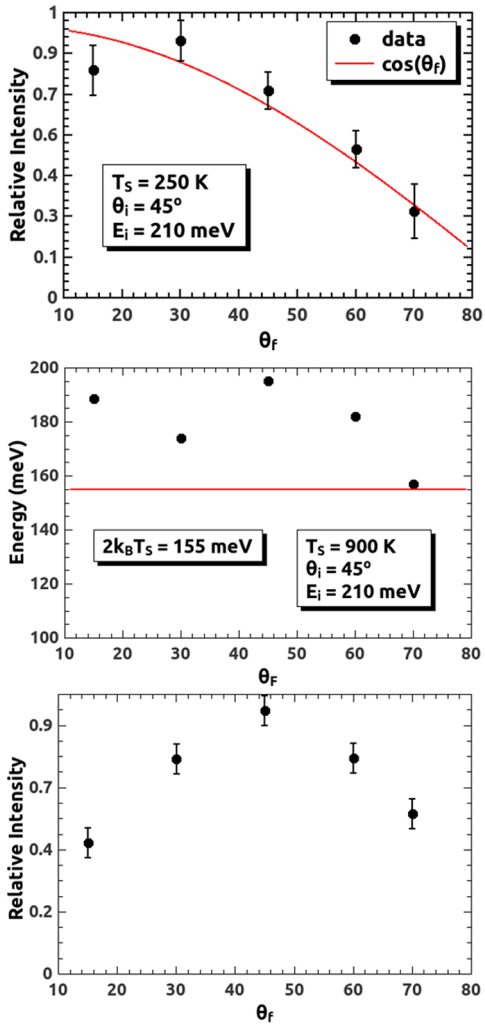

Figure 8. Top panel: intensities for the scattering of the 210 meV beam when T_S = 250 K. Only one Maxwell−Boltzmann distribution function was used, and the average energy was ∼48 meV. The red line is the fit of the data to a $\cos(\theta_f)$ intensity distribution. Middle and bottom panels: energies and relative intensities for the scattering of the 210 meV beam when T_S = 250 K. The red line in the energy plot is for $E = 2k_BT_S$.

range to times after the chopper had blocked the beam. The red line in Figure 4 is an example of the results of this fitting process. With the values at different surface temperatures, it is possible to make an Arrhenius plot with

$$1/\tau \propto \exp(-E_d/k_BT_S) \quad (1)$$

where E_d is the DMMP desorption energy. The result is shown in Figure 4, and E_d = 290 ± 60 meV (28 ± 6 kJ/mol), a reasonable value for a physisorbed molecule. It is about half of the value that Hegde et al. measured for monolayer carbon adsorbed on Rh(100),[4] and also about half of what was seen on amorphous silica,[26] but both of these studies saw a higher desorption temperature. An important point is that residence time decreases rapidly with T_S, being only a few microseconds at a still cryogenic temperature of 235 K.

A last set of experiments examined the gas−surface interaction for surface temperatures between 250 and 900 K. These involved measuring the DMMP scattering as a function of surface temperature and final angle (all of the data were taken with θ_i = 45°). This was done with a mixture of TOF measurements and total intensity measurements using square-wave chopping. The total intensity measurements give the best signal-to-noise ratios, but if the translational energy of the scattered molecules varies as a function of θ_f, it is important to measure the velocity so that the relative intensities from the number-density detector can be converted to flux.

Figure 5 shows some examples of TOF spectra. These were taken with the postcollision cross-correlation chopper. The resultant spectra were deconvoluted and then fit with shifted Maxwell−Boltzmann distributions:

$$f(v) \propto v^3 \times \exp(-([v - v_0]/\alpha)^2) \quad (2)$$

The nonlinear least-squares routine uses three adjustable parameters for each distribution: the intensity, the stream velocity, v_0, and α, which is a measure of the width ($\alpha^2 = 2k_BT/m$, where T is the internal temperature of the distribution). Both of the spectra shown in Figure 5 were fit with the sum of two velocity distributions.

Figures 6 and 7 summarize the results for an incident translational energy of 730 meV. For the lower surface temperatures, 250 and 400 K, there are two distinct fractions with different final translational energies. This bimodal energy distribution is quite common,[27,28] though much of the data are for rare gases,[29−32] where there is no internal structure, or for a diatomic such as NO[33] or HCl.[34] However, qualitatively, the intensity and translational energy of the DMMP scattering is similar. The low energy fraction, the trapping−desorption component, has an angular intensity distribution that varies as $\cos(\theta_f)$, shown by the blue lines through the points. The final average energy is nearly $2k_BT_S$ and is independent of θ_f. The incident molecules transiently trapped on the surface long enough that the molecules were nearly accommodated to the surface temperature and no longer have a memory of the incident momentum. This accommodation only requires a few picoseconds near the surface.[31,32] Though we are only probing in-plane scattering, the intensity distribution likely covers the entire 2π steradians above the plane of the surface.

At glancing angles, the in-plane scattering also has a component with translational energies of about half the incident beam, and the intensity is peaked toward glancing angles greater than specular. This component, from the direct-inelastic scattering, has lost more of the initial momentum perpendicular to the surface than parallel to it but retains much of its initial translational energy. The interaction with the surface is probably only a single bounce, and so the time near the MLG surface is only a few picoseconds. The ratio of trapping−desorption to direct-inelastic scattering decreases with increasing surface temperature. This has also been observed for other systems.[32,35]

Figures 8 and 9 show results for two other beam energies: 210 and 1520 meV. The lower energy beam used Ar as the carrier gas, and the higher energy beam used a higher backing pressure of He (19.7 psia versus 7 psia for the 730 meV DMMP). Both of these beams showed evidence of clustering; both had an m/e = 218 component. However, the results are similar to those of the 730 meV beam, with a significant trapping−desorption component at T_S = 250 K, and principally direct-inelastic scattering at T_S = 900 K.

So far, we have made no mention of the internal energy distribution and how it is affected by interaction with the surface. For the electron energies we used in our ionizer, 95 eV, large organic molecules will produce many different charged fragments. Moreover, we know that the internal energy distribution can affect the cracking pattern when a neutral is ionized.[36,37] Therefore, it should be possible to make some inference of the

DOI: 10.1021/acs.jpca.5b12419
J. Phys. Chem. A 2016, 120, 4863−4871

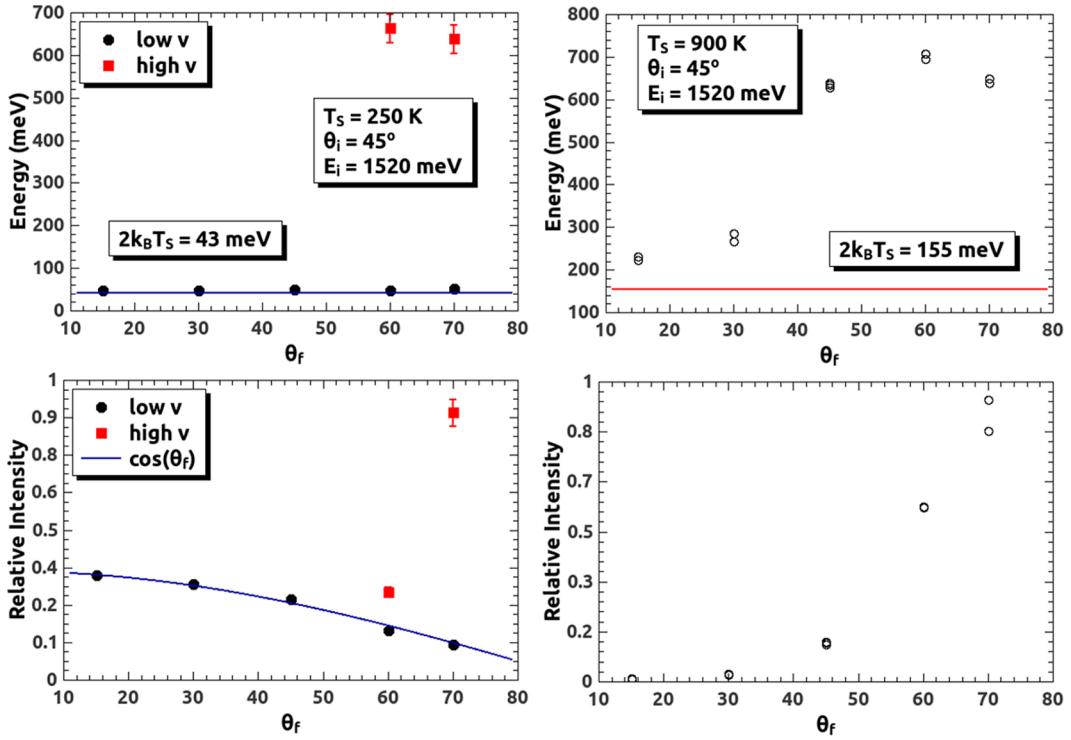

Figure 9. Top panels: average final translational energy as a function of θ_f. Bottom panels: scattered intensity as a function of θ_f. For any final angles where the TOF distributions were bimodal, two points are plotted, with the higher energy in red. The line through the intensities is $\cos(\theta_f)$. The lines in the energy plots are for $E = 2k_BT_S$.

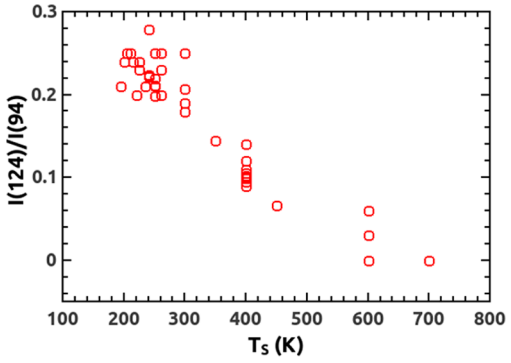

Figure 10. Ratio of the $m/e = 124$ to $m/e = 94$ intensities as a function of the surface temperature.

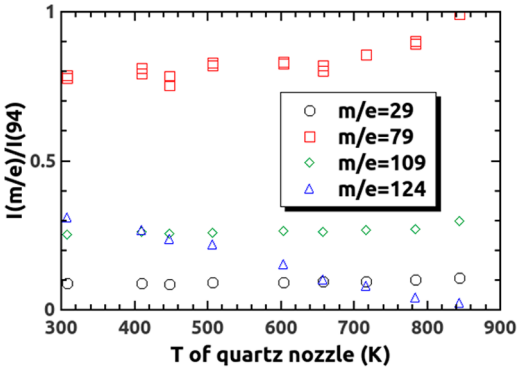

Figure 11. Intensity of some of the mass fragments measured in the QMS referenced to the intensity of $m/e = 94$ as a function of the quartz nozzle temperature. The $m/e = 29$ fragment would be the most intense formaldehyde fragment in an electron-bombardment ionizer; there is also some $m/e = 29$ from the fragmentation of DMMP in the ionizer.

internal energy of a molecule leaving the surface by examining the cracking pattern. Liang et al.,[16] who used photoionization instead of electron impact, saw the relative intensities of the various fragments of DMMP change with the temperature of their pyrolysis tube, even before there was any decomposition of the DMMP. Notably, the ratio of $m/e = 124$ to $m/e = 94$ decreased as the temperature increased. Figure 10 shows the ratio of the intensities that we observed for $m/e = 124$ (the parent peak) to $m/e = 94$. The data are primarily from measuring the total intensity, because the $m/e = 124$ signal is so small. However, for the conditions where we made TOF measurements, there was no difference in the velocities for the two masses; we are fairly certain that all of the dissociation products were formed in the ionizer. Most of the data are for nearly normal final angles, though some are for glancing. Included are incident translational energies from 0.2 to 3 eV, and beams with significant DMMP clustering. As mentioned, the ratio of $m/e = 124$ to $m/e = 94$ was 0.25 from the 303 K nozzle. This is consistent with the scattering data for a surface temperature of around 300 K. By $T_S = 400$ K, this ratio is halved. For molecules leaving the surface near the normal direction, the translational energy and intensity distribution indicate nearly complete thermal accommodation. It seems probable that the internal energy distribution warmed as it approached equilibration with the MLG surface temperature, and that is our interpretation of the decrease in the $m/e = 124$ to $m/e = 94$ ratio. By $T_S = 600$ K, the ratio is nearly zero, allowing us to infer that the internal temperature has probably increased even more.

To test the hypothesis that the change in the cracking pattern was due to a change in the internal energy and not to reaction, we did some measurements using a heated quartz tube. Liang et al.[16]

DOI: 10.1021/acs.jpca.5b12419
J. Phys. Chem. A 2016, 120, 4863−4871

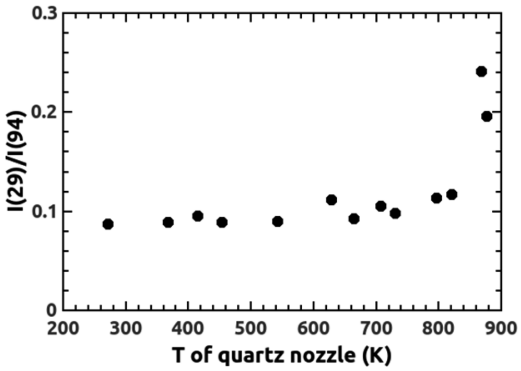

Figure 12. Intensity of some of the m/e = 29 mass fragment referenced to the intensity of m/e = 94 as a function of the quartz nozzle temperature. The m/e = 29 fragment would be the most intense formaldehyde fragment,; there is also some m/e = 29 from the fragmentation of DMMP in the ionizer. At a temperature greater than 850 K, the m/e = 29 to m/e = 94 ratio increases.

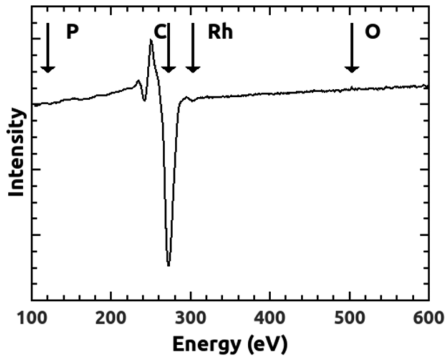

Figure 13. Auger electron spectrum of an MLG surface after long exposure (ca. 50 h) to DMMP at surface temperatures between 250 and 600 K. Arrows indicate the expected positions of the principle Auger features for phosphorus, oxygen, carbon, and rhodium.

used a pyrolyis reactor[38] (short contact times in a heated SiC tube and the absence of oxygen) to examine the thermal decomposition of DMMP. They did not see appreciable decomposition until the temperature of the tube was ~1000 K. The quartz tube should be equally inert for DMMP decomposition. The tube had a 0.04 in. hole and was resistively heated by a coil of heater wire (Thermocoax, 1 Nc I 10) tightly wound around the circumference. Temperature was measured with a type K thermocouple, calibrated using pure Ar to make either an effusive or supersonic molecular beam. The DMMP beam was made by bubbling low pressure He or Ar (<10 Torr) through a room temperature reservoir of the liquid DMMP. The measurements were all done on the direct beam. The results are shown in Figure 11, where the intensities for different m/e are shown as a function of the quartz nozzle temperature, all referenced to the measured intensity of m/e = 94. Most notably, the m/e = 124 to m/e = 94 ratio drops significantly with increasing temperature. Liang et al.[16] found that formaldehyde was one of the main products of decomposition. In our detector, the principal fragment should occur at m/e = 29. This is also a minor component due to the cracking of DMMP. So, we see some m/e = 29 at all temperatures, but within our experimental error, *there is no increase relative to* m/e = 94 expected if there was the formation of formaldehyde in the nozzle. The maximum temperature was ~850 K, well below the temperature where decomposition was expected.

To further test the internal energy versus decomposition hypothesis, we exposed the cooled (T_S = 130 K) MLG surface to a beam of DMMP from the quartz nozzle, with the nozzle temperature at either 305 or 832 K. TPD spectra were then taken while monitoring m/e = 79, 94, and 124. For the 305 K beam the m/e = 79 to m/e = 94 and m/e = 124 to m/e = 94 ratios were 0.84 and 0.25. At a nozzle temperature of 832 K, the same ratios were 0.83 and 0.26, identical within our experimental error. This is fairly definitive evidence that at the temperatures we used, the change in the detected fragments is due to internal energy changes and not DMMP decomposition.

With some modification of the quartz nozzle heating, we were able to reach almost 900 K. The ratio of m/e = 29 to m/e = 94 is shown in Figure 12, where there is finally a clear increase in the relative intensity of m/e = 29 at a nozzle temperature between 850 and 900 K. TOF spectra taken below 850 K showed that the m/e = 29 and m/e = 94 signals had the same velocity, as would be expected if their formation was in the ionizer. At higher temperatures, the m/e = 29 signal was appreciably faster than m/e = 94. We attribute this to formaldehyde formation in the heated quartz tube. This temperature is lower than reported by Liang et al.[16] but is near the maximum graphite surface temperature that we studied.

We also did a few experiments looking for excess m/e = 29 in the scattering at T_S < 1000 K but did not detect any. Our MLG surfaces cannot be heated any higher because the carbon will dissolve back into the bulk. We ran experiments for many days using the same MLG overlayer and measured the Auger spectrum. A result after several days of exposure at elevated temperatures is shown in Figure 13; there is no oxygen or phosphorus signal. Though we cannot rule out the possibility of a small level of reaction, we essentially see no evidence for decomposition from the results of our comprehensive experiments. It is important to point out that at the highest surface temperatures, there were only a few bounces with the surface, whereas in the quartz tube there were many collisions with both the tube walls and other molecules (0.5 in. diameter tube, ~2 in. long oven, a few Torr pressure). This can greatly enhance the probability of reaction.

CONCLUSIONS

We explored the interaction of a molecular beam of a chemical warfare agent simulant, DMMP, with a chemically inert surface, MLG. The experiments were done at surface temperatures between 120 and 900 K. At the lowest temperatures, the DMMP is adsorbed, with the molecules next to the carbon surface held slightly more strongly than the bulk, multilayer DMMP that grows with continued dosing. We measured the desorption energy for submonolayer coverage using modulated beam techniques and found a value of 290 meV (28 kJ/mol). The surface residence time is only a few microseconds by T_S = 235 K.

At higher surface temperatures, where the residence times are very short, we measured the scattering of the DMMP as a function of angle and translational kinetic energy using TOF techniques. For T_S = 250 K, and DMMP translational kinetic energies between 200 and 1500 meV, much of the incident flux has been nearly accommodated with the surface temperature, as evidenced by the dominance of trapping−desorption scattering, characterized by observing a final translational kinetic energy of $\sim 2k_B T_S$, and an intensity distribution that goes as $\cos(\theta_f)$. The internal energy also seems to be accommodating as well. As the surface temperature increases, the scattering transitions to direct-inelastic reflection, where much of the incident translational

DOI: 10.1021/acs.jpca.5b12419
J. Phys. Chem. A 2016, 120, 4863−4871

energy is retained, and the intensity of the scattering peaks toward forward glancing final angles.

The results shown in this paper demonstrate the efficacy of using kinetic energy controlled molecular beams to probe in great detail the interactions of rather complex organic molecules with well-defined surfaces, extending in several ways our fundamental understanding of how the scattering dynamics for such systems crossover from trapping−desorption to direct-inelastic scattering.

This study has yielded critically needed information about the interaction of a relatively volatile organophosphate chemical warfare simulant, DMMP, with an inert surface, multilayer graphene. The experiments outlined in this paper contribute to our understanding of the behavior of a dispersed agent, such as sarin, with a chemically inert surface. These results indicate, importantly, that simulations that model the dispersal of chemical warfare agents using many common interfaces in the environment need to account for the multiple bounce trajectories of the impinging molecules.

AUTHOR INFORMATION

Corresponding Author

*S. J. Sibener. Email: s-sibener@uchicago.edu. Tel: 773-702-7193.

Notes

The authors declare no competing financial interest.

ACKNOWLEDGMENTS

This work was sponsored by the Defense Threat Reduction Agency (DTRA) under Grant HDTRA1-11-1-0001. Infrastructure support from the NSF-Materials Research Science and Engineering Center at The University of Chicago, Grant No. NSF-DMR-14-20709, is also gratefully acknowledged.

REFERENCES

(1) Kim, K.; Tsay, O. G.; Atwood, D. A.; Churchill, D. G. Destruction and Detection of Chemical Warfare Agents. *Chem. Rev.* **2011**, *111*, 5345−5403.

(2) Butrow, A. B.; Buchanan, J. H.; Tevault, D. E. Vapor Pressure of Organophosphorus Nerve Agent Simulant Compounds. *J. Chem. Eng. Data* **2009**, *54*, 1876−1883.

(3) Ekerdt, J.; Klabunde, K.; Shapley, J.; White, J.; Yates, J. Surface-Chemistry of Organo-Phosphorus Compounds. *J. Phys. Chem.* **1988**, *92*, 6182−6188.

(4) Hegde, R.; Greenlief, C.; White, J. Surface-Chemistry of Dimethyl Methylphosphonate on Rh(100). *J. Phys. Chem.* **1985**, *89*, 2886−2891.

(5) Guo, X.; Yoshinobu, J.; Yates, J. Decomposition of an Organophosphonate Compound (Dimethyl Methylphosphonate) on the Ni(111) and Pd(111) Surfaces. *J. Phys. Chem.* **1990**, *94*, 6839−6842.

(6) Smentkowski, V.; Hagans, P.; Yates, J. Study of the Catalytic Destruction of Dimethyl Methylphosphonate - Oxidation Over Mo(110). *J. Phys. Chem.* **1988**, *92*, 6351−6357.

(7) Ratliff, J. S.; Tenney, S. A.; Hu, X.; Conner, S. F.; Ma, S.; Chen, D. A. Decomposition of Dimethyl Methylphosphonate on Pt, Au, and Au-Pt Clusters Supported On. TiO_2(110). *Langmuir* **2009**, *25*, 216−225.

(8) Gordon, W. O.; Tissue, B. M.; Morris, J. R. Adsorption and Decomposition of Dimethyl Methylphosphonate on Y_2O_3 Nanoparticles. *J. Phys. Chem. C* **2007**, *111*, 3233−3240.

(9) Panayotov, D. A.; Morris, J. R. Uptake of a Chemical Warfare Agent Simulant (DMMP) on TiO_2: Reactive Adsorption and Active Site Poisoning. *Langmuir* **2009**, *25*, 3652−3658.

(10) Panayotov, D. A.; Morris, J. R. Thermal Decomposition of a Chemical Warfare Agent Simulant (DMMP) on TiO_2: Adsorbate Reactions with Lattice Oxygen as Studied by Infrared Spectroscopy. *J. Phys. Chem. C* **2009**, *113*, 15684−15691.

(11) Tesfai, T. M.; Sheinker, V. N.; Mitchell, M. B. Decomposition of Dimethyl Methylphosphonate (DMMP) on Alumina-Supported Iron Oxide. *J. Phys. Chem. B* **1998**, *102*, 7299−7302.

(12) Panayotov, D. A.; Morris, J. R. Catalytic Degradation of a Chemical Warfare Agent Simulant: Reaction Mechanisms on TiO2-Supported Au Nanoparticles. *J. Phys. Chem. C* **2008**, *112* (19), 7496−7502.

(13) Christmann, K. (Klaus). *Introduction to Surface Physical Chemistry*; Steinkopff Verlag, Springer-Verlag: Darmstadt, New York, 1991.

(14) Ferguson-McPherson, M. K.; Low, E. R.; Esker, A. R.; Morris, J. R. Sorption of Dimethyl Methylphosphonate within Langmuir-Blodgett Films of Trisilanolphenyl Polyhedral Oligomeric Silsesquioxane. *J. Phys. Chem. B* **2005**, *109*, 18914−18920.

(15) Bertilsson, L.; Engquist, I.; Liedberg, B. Interaction of Dimethyl Methylphosphonate with Alkanethiolate Monolayers Studied by Temperature-Programmed Desorption and Infrared Spectroscopy. *J. Phys. Chem. B* **1997**, *101*, 6021−6027.

(16) Liang, S.; Hemberger, P.; Neisius, N. M.; Bodi, A.; Gruetzmacher, H.; Levalois-Gruetzmacher, J.; Gaan, S. Elucidating the Thermal Decomposition of Dimethyl Methylphosphonate by Vacuum Ultraviolet (VUV) Photoionization: Pathways to the PO Radical, a Key Species in Flame-Retardant Mechanisms. *Chem. - Eur. J.* **2015**, *21*, 1073−1080.

(17) Holtzclaw, J. R.; Wyatt, J. R.; Campana, J. E. Structure and Fragmentation of Dimethyl Methylphosphonate and Trimethyl Phosphite. *Org. Mass Spectrom.* **1985**, *20*, 90−97.

(18) Comsa, G.; David, R.; Schumacher, B. J. Magnetically Suspended Cross-correlation Chopper in Molecular Beam-Surface Experiments. *Rev. Sci. Instrum.* **1981**, *52*, 789−796.

(19) Gibson, K. D.; Sibener, S. J. Helium Atom Scattering from Graphene Grown on Rh(111). *J. Phys. Chem. C* **2014**, *118*, 29077−29083.

(20) Dong, G. C.; van Baarle, D. W.; Rost, M. J.; Frenken, J. W. M. Graphene Formation on Metal Surfaces Investigated by in-Situ Scanning Tunneling Microscopy. *New J. Phys.* **2012**, *14*, 053033.

(21) Rut'kov, E.; Kuz'michev, A.; Gall', N. Carbon Interaction with Rhodium Surface: Adsorption, Dissolution, Segregation, Growth of Graphene Layers. *Phys. Solid State* **2011**, *53*, 1092−1098.

(22) McCarty, K. F.; Feibelman, P. J.; Loginova, E.; Bartelt, N. C. Kinetics and Thermodynamics of Carbon Segregation and Graphene Growth on Ru(0001). *Carbon* **2009**, *47*, 1806−1813.

(23) Jackson, D. C.; Gallon, T. E.; Chambers, A. A Model for the Auger Electron Spectroscopy of Systems Exhibiting Layer Growth, and Its Application to the Deposition of Silver on Nickel. *Surf. Sci.* **1973**, *36*, 381−394.

(24) Jones, R. H.; Olander, D. R.; Siekhaus, W. J.; Schwarz, J. A. Investigation of Gas−Solid Reactions by Modulated Molecular Beam Mass Spectrometry. *J. Vac. Sci. Technol.* **1972**, *9*, 1429−1441.

(25) Engel, T. A Molecular Beam Investigation of He, CO, and O_2 Scattering from Pd(111). *J. Chem. Phys.* **1978**, *69*, 373−385.

(26) Wilmsmeyer, A. R.; Uzarski, J.; Barrie, P. J.; Morris, J. R. Interactions and Binding Energies of Dimethyl Methylphosphonate and Dimethyl Chlorophosphate with Amorphous Silica. *Langmuir* **2012**, *28*, 10962−10967.

(27) Arumainayagam, C. R.; Madix, R. J. Molecular Beam Studies of Gas-Surface Collision Dynamics. *Prog. Surf. Sci.* **1991**, *38*, 1−102.

(28) Barker, J. A.; Auerbach, D. J. Gas—surface Interactions and Dynamics; Thermal Energy Atomic and Molecular Beam Studies. *Surf. Sci. Rep.* **1984**, *4*, 1−99.

(29) Andersson, P.; Nagard, M.; Bolton, K.; Svanberg, M.; Pettersson, J. Dynamics of Argon Collisions with Water Ice: Molecular Beam Experiments and Molecular Dynamics Simulations. *J. Phys. Chem. A* **2000**, *104*, 2681−2688.

(30) Bolton, K.; Svanberg, M.; Pettersson, J. Classical Trajectory Study of Argon-Ice Collision Dynamics. *J. Chem. Phys.* **1999**, *110*, 5380−5391.

(31) Gibson, K. D.; Isa, N.; Sibener, S. J. Experiments and Simulations of Hyperthermal Xe Interacting with an Ordered 1-Decanethiol/Au(111) Monolayer: Penetration Followed by High-Energy, Directed Ejection†. *J. Phys. Chem. A* **2006**, *110*, 1469−1477.

DOI: 10.1021/acs.jpca.5b12419
J. Phys. Chem. A 2016, 120, 4863−4871

(32) Gibson, K. D.; Isa, N.; Sibener, S. J. Experiments and Simulations of Ar Scattering from an Ordered 1-decanethiol−Au(111) Monolayer. *J. Chem. Phys.* **2003**, *119*, 13083.
(33) Rettner, C.; Kimman, J.; Auerbach, D. Inelastic-Scattering of No from Ag(111) - Internal State, Angle, and Velocity Resolved Measurements. *J. Chem. Phys.* **1991**, *94*, 734−750.
(34) Andersson, P. U.; Någård, M. B.; Pettersson, J. B. C. Molecular Beam Studies of HCl Interactions with Pure and HCl-Covered Ice Surfaces. *J. Phys. Chem. B* **2000**, *104*, 1596−1601.
(35) Mullins, C. B.; Rettner, C. T.; Auerbach, D. J.; Weinberg, W. H. Variation of the Trapping Probability of Ar on Pt(111) with Kinetic Energy and Angle of Incidence: The Changing Role of Parallel Momentum with Surface Temperature. *Chem. Phys. Lett.* **1989**, *163*, 111−115.
(36) Vekey, K. Internal Energy Effects in Mass Spectrometry. *J. Mass Spectrom.* **1996**, *31*, 445−463.
(37) Kolodney, E.; Tsipinyuk, B.; Budrevich, A. The Thermal-Energy Dependence (10−20 Ev) of Electron-Impact Induced Fragmentation of C-60 in Molecular-Beams - Experiment and Model-Calculations. *J. Chem. Phys.* **1995**, *102*, 9263−9275.
(38) Kohn, D. W.; Clauberg, H.; Chen, P. Flash Pyrolysis Nozzle for Generation of Radicals in a Supersonic Jet Expansion. *Rev. Sci. Instrum.* **1992**, *63*, 4003−4005.

DOI: 10.1021/acs.jpca.5b12419
J. Phys. Chem. A 2016, 120, 4863−4871